Article

Seakeeping tests of a FOWT in wind and waves: an analysis of dynamic coupling effects and their impact on the predictions of pitch motion response.

Giovanni A. Amaral [1], Pedro C. Mello [1]*, Lucas H. S. do Carmo [1], Izabela F. Alberto[1], Edgard B. Malta[2], Alexandre N. Simos[1], Guilherme R. Franzini[1], Hideyuki Suzuki[3] and Rodolfo T. Gonçalves[3]

[1] Escola Politécnica, University of São Paulo; São Paulo, SP, Brazil
[2] Technomar – Engenharia Oceânica; São Paulo, SP, Brazil
[3] OSPL – Ocean Space Planning Laboratory; The Univeristy of Tokyo; Tokyo, Japan
* Correspondence: pcmello@usp.br

Abstract: The present work highlights some of the dynamic couplings observed in a series of tests performed in a wave basin with a scaled-model of a FOWT with semi-submersible substructure. The model was moored by means of a conventional chain catenary system and an actively controlled fan was used for emulating the thrust loads during the tests. A set of wave tests comprising regular and irregular waves was done for different wave angles and wind velocities. The experimental records illustrate the main coupling effects involved and how they affect the FOWT motions in waves, especially when the floater presents a non-negligible tilt angle.. In addition, an analysis of the frequency-domain dynamic model was made in order to evaluate its ability to capture these effects properly. The influence of different modes of fan response, floater trim angles (changeable with ballast compensation) and variations of the mooring stiffness with the offsets were investigated in the analysis. Results attest that significant changes in the FOWT responses may indeed arise from coupling effects, thus indicating that caution must be taken when simplifying the hydrodynamic frequency-domain models often used as a basis for the simulation of FOWTs in waves and in in optimization procedures for the design of the floater and mooring lines.

Keywords: FOWT dynamics; seakeeping model tests; dynamic coupling effects; pitch motion response.

1. Introduction

Parametric optimization of floater and moorings is a procedure frequently employed in the first stages of the design of a new Floating Offshore Wind Turbine (FOWT). In this approach, simplified models are often used for predicting the dynamics of the system while ensuring that the process will meet the time constraints imposed by the design. A trade-off is then established between the accuracy of force and motion predictions and the computational demand of an optimization procedure. In this context, the predictions of motions in waves is generally based on pre-computed hydrodynamic loads or motion transfer functions obtained from radiation/diffraction codes [4–6]. Moreover, hydrodynamic coefficients derived from panel methods are also the basis for sea-keeping time-domain simulations that consider the coupled dynamics of floater, rotor and mooring lines, considering not only the wave-frequency motions but also the slow-motions induced by second-order effects.

Nevertheless, some of the main characteristics of a typical FOWT, such as the light hull structures, make their dynamics more susceptible to the effects induced by couplings with the mooring lines and, of course, the rotor loads, and part of these effects may arise from external causes that may be difficult to predict in a proper manner when preparing the hydrodynamic model. This may be even more important for concepts that don't make use of active ballast compensation, a trend that may be favored as the turbines become more tolerant with respect inclinations and nacelle accelerations.

 doi:10.20944/preprints202101.0071.v1

The present work is part of a R&D project conducted cooperatively by the University of São Paulo and the University of Tokyo, in which different FOWT concepts were proposed and evaluated for operation in a particular site in the Brazilian coast [1–3]. Using the NREL 5MW turbine [17] as a reference for the wind turbine, one of the main objectives of the project was to develop, calibrate and test the performance of a computational tool designed for parametric optimization of the floater and mooring system geometries. The core of such tool consists in a simplified dynamic model intended for predicting the wave-frequency motions of each particular geometric configuration in an automated and expeditious way. For that, the software was integrated with WAMIT®, together with a procedure for estimating the viscous damping levels. In its essence, the procedure is similar to previous works available in the literature, as for example [4–6].

Several model tests were done during the project, in different stages of the design and with different purposes. In the present work, the chosen floater was consisted of four vertical columns with heave plates (a central column that supports the tower and three orbital columns) and it was moored in the wave basin by means of three catenary lines. An active fan was used to emulate the rotor thrust during the tests, according to the loads predicted by a BEM (blade element momentum) code integrated to the tests in a software-in-the-loop scheme, a procedure similar to the ones adopted, for example, by [7–10].

In the tests, two different wind speeds were used, a mild wind condition in the below-rated regime and a more intense one, corresponding to the maximum rotor thrust. In both cases, no active blade pitch control was considered, but the thrust was corrected by the BEM model according to apparent wind velocities induced by the model motions.

Another important aspect concerns the ballast compensation. The FOWT concept used in the tests includes an active ballast control for adjusting the floater trim. For the tests, however, no active ballast control was considered, but two different strategies were adopted: in the first one, a correction of the ballast mass was made in order to compensate most of the tilt induced by the rotor thrust; in the second approach, no compensation was made, allowing situations with somewhat çarge tilt angles, especially in the condition of maximum thrust (approximately 10 degrees).

As one may anticipate, this set of variations in the rotor loads and in the floater attitude (trim angles) resulted in significant changes in the FOWT motion response. These changes were detectable in the decay tests as well as in the wave tests, and the main objective in the analyses presented ahead is to evaluate the effects that dominated the variations and our ability to predict then when using simplified frequency-domain models.

Firstly, one must take into account the fluctuations of the rotor thrust due to the tower motions. In this respect, a series of previous works are available in literature, which deal with this problem and explain very well most of the consequences that should be expected. For instance, [11] models the damping effect induced by the thrust variations, and [12] observe that an “apparent inertia” may also result for conditions when the blade pitch is controlled, due to a phase shift between the thrust response and the nacelle accelerations. On the other hand, the floater tilt can also impose significant changes, especially in the FOWT pitch motion response. One of the main issues in this case is the heave-pitch dynamic coupling that appears as a result of the mean trim angle. Here, both hydrodynamic effects and mooring line tensions may play an important role. Finally, there are the general variations of the mooring stiffness due to the horizontal offsets of the floater, which may potentially contribute to the changes observed in the motions. This is the case for the low-frequency surge/sway motions in particular, a fact already observed by [12].

In the next sections, all these possible causes of change in the motions response will be explored and attempts to quantify the external effects (stiffness, damping) in the frequency-domain hydrodynamic model will be evaluated by confronting the predictions with the to experimental results obtained in the wave basin. First, however, a description of the model and experimental setup will be made, followed by the main considerations adopted in wind turbine characterization and the hydrodynamic model of the FOWT. Section 3 will provide the main results from both numerical and

Preprints (www.preprints.org) | NOT PEER-REVIEWED | Posted: 5 January 2021 doi:10.20944/preprints202101.0071.v1

physical tests and a discussion on the level of agreement obtained in the predictions. Finally, the main conclusions derived from this analysis will be summarized in Section 4.

2. Materials and Methods

This section first presents the Jappaku FOWT [1] floating structure and its mooring system, which is followed by a description of the experimental setup adopted in the model tests and the presentation of the main features of the radiation-diffraction numerical model employed for the prediction of its responses in waves.

2.1. FOWT geometry and mooring system

The Jappaku FOWT floating structure consists of a semisubmersible hull with a central column that supports the turbine tower and three orbital columns disposed in a triangular shape. The central column presents a larger diameter if compared to the orbital ones. For the purpose of the present model tests, the columns were connected by a set of deck bracings, as presented in Fig. 1. Following the developments presented in a previous work [2], heave plates are adopted in each column as a means to tune the natural periods of motions and to increase the viscous damping levels in resonant conditions. Tab. 1 brings the main properties of the Jappaku FOWT in both, full- and model- scales (1:80). Ballast weights were distributed in the model in order to match the position of the center of gravity and the inertias of the full-scale FOWT with the help of commercial software Edtools® [13].

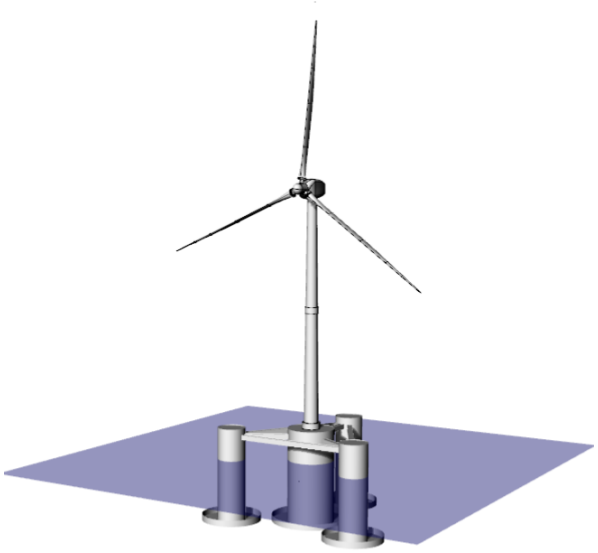

Figure 1. Details of the Jappaku FOWT.

Table 1. Jappaku FOWT hull main properties.

	Full-scale	Model-scale (1:80)
Diameter of center column	15 m	187.5 mm
Diameter of side columns	9 m	112.5 mm
Draft	20 m	250 mm
Heave plate width	4 m	50 mm
Diameter of central column's heave plate	25 m	312.5 mm
Diameter of side columns' heave plate	19 m	237.5 mm
Displacement	7351 ton	14.35 kg
CG (from bottom)	14 m	175 mm

The FOWT model was moored in the basin by means of three catenary mooring lines, as presented in Fig. 2. Each mooring line was composed by two different segments: chain (bottom) and polyester

Preprints (www.preprints.org) | NOT PEER-REVIEWED | Posted: 5 January 2021 doi:10.20944/preprints202101.0071.v1

wire (upper segment). Fairleads were located at the bottom of the side columns, under the heave plates, at a radius corresponding in full-scale to 30 m from the axis of the central column. Water depth in the basin corresponded to 302.8 m in full-scale, and the anchor radius was 543.1 m. Tab. 2 shows the mooring system main properties in both full and model-scales.

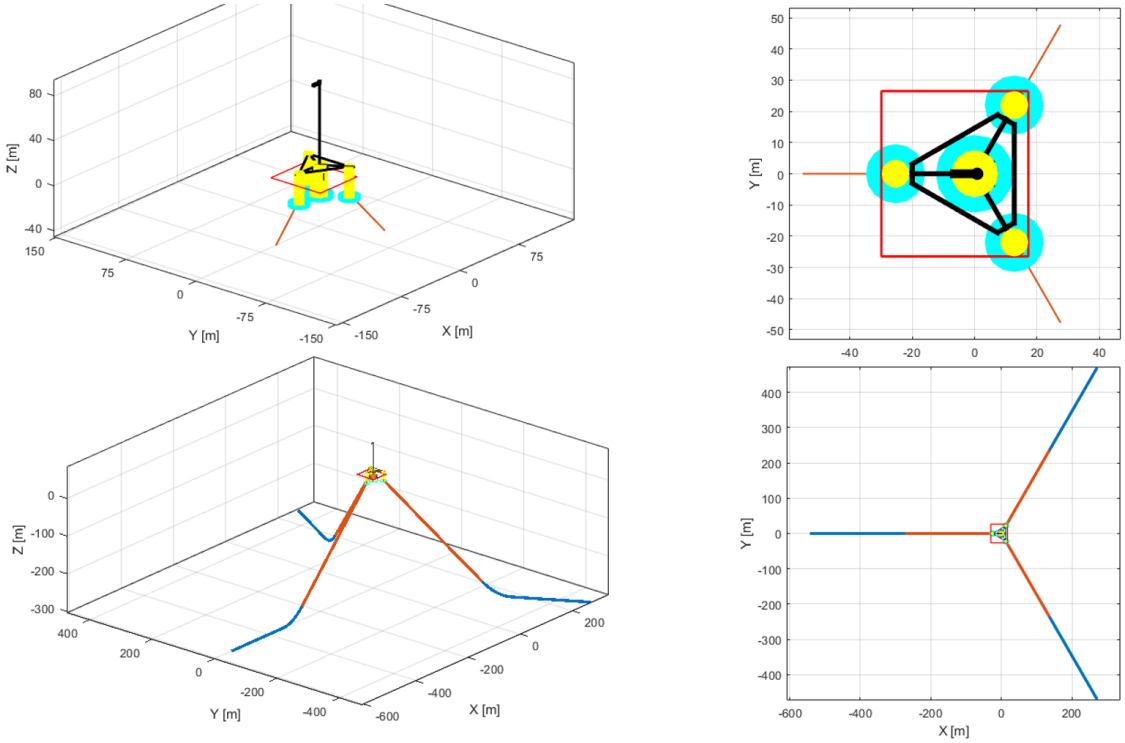

Figure 2. Jappaku FOWT mooring system by Edtools® software in full-scale.

Table 2. Jappaku FOWT mooring system main properties.

	Full-scale	Model-scale (1:80)
Number of mooring lines	3	3
Anchors' depth	302.8 m	3785 mm
Anchors' radius from center	534.1 m	6789 mm
Fairleads' depth	20 m	250 mm
Fairleads' radius	30 m	375 mm
Bottom segment material	Chain	Chain
Bottom segment length	280 m	3500 mm
Bottom segment equivalent submerged weight	9.21 kN/m	1.44 N/m
Upper segment material	Polyester	Polyester
Upper segment length	347.6 m	4345 mm
Upper segment equivalent submerged weight	0.04 kN/m	0.01 N/m

2.2. Experimental setup

The experimental tests were conducted at wave basin of the Numerical Offshore Tank Laboratory (TPN) of the University of São Paulo (Fig. 3). The facility consists of a squared 14 m × 14 m × 4 m (length, width, depth) basin with flap-type wave makers distributed all around the basin, which are also responsible for active wave absorption (complete information on the ocean basin can be found in [14]). The scale factor adopted for the tests was 1:80, following previous experimental studies performed with the same model [2]. In this new set of tests, the main purposes were to evaluate the catenary anchoring systems and the effects of the wind emulated by an actuator in a software-in-the-loop (SIL) approach.

Preprints (www.preprints.org) | NOT PEER-REVIEWED | Posted: 5 January 2021 doi:10.20944/preprints202101.0071.v1

The experimental campaign included regular and irregular wave tests. In the present paper, only the tests performed for characterizing the first-order motions of the FOWT will be addressed. These tests involved regular (monochromatic) and white-noise waves, performed with and without wind emulation. The RAOs obtained from both approaches are compared and presented a fair agreement. For this reason, and for the sake of conciseness, the discussions ahead will be restricted to the results obtained with the white-noise waves. The white-noise wave had a duration of 1315 s with energy ranging from 6.4 s to 27 s. The significant wave height was equivalent to 1.9 m with constant energy distribution. Fig. 4 presents the wave record obtained in the tank and the PSD derived from it, for illustration purposes.

A set of two wave probes (WP) was used to measure the waves during the tests: one was positioned ahead of the model location (meaning waves hit this WP before reaching the model) and one was placed sideways. A third WP was positioned at the model location during wave calibration as wave reference and later removed for the model tests. The model motions were measured using a Qualisys® optical tracking system with cameras positioned above the model in the instrumentation bridge. Four stationary infrared cameras were used to track a set of six passive markers attached to the model structure. The redundancy of cameras and markers was used to provide accuracy and reliability for the motion measurements, with residual measurement for each marker being less than 1.0 mm. The sampling frequency adopted during the measurements was 100 Hz.

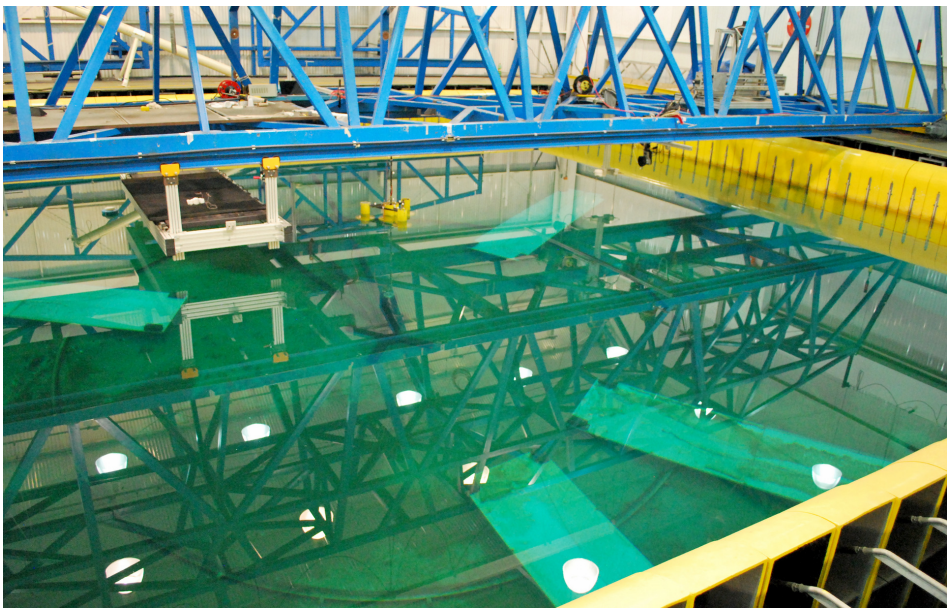

Figure 3. Ocean basin of CH-TPN.

2.3. Wind emulation by Software in the loop (SIL)

The wind was emulated during the tests by using a SIL approach. For that, a previously developed algorithm that computes the aerodynamic loads on the rotor based on BEMT was integrated in the tests. The position data recorded by the camera tracking system and the motion velocities computed in 6-dof served as input to the SIL model. The computer then sent the required aerodynamic thrust calculated in each time sample to a wind actuator composed of a computer interface, a motor driver ESC (electronic speed control) and, finally, to a brushless motor with a propeller.

The BEMT code with the model of the NREL 5MW turbine was implemented in C++ and compiled for running in MATLAB (details on the BEMT routine can be found in [15] and [16]).

Preprints (www.preprints.org) | NOT PEER-REVIEWED | Posted: 5 January 2021 doi:10.20944/preprints202101.0071.v1

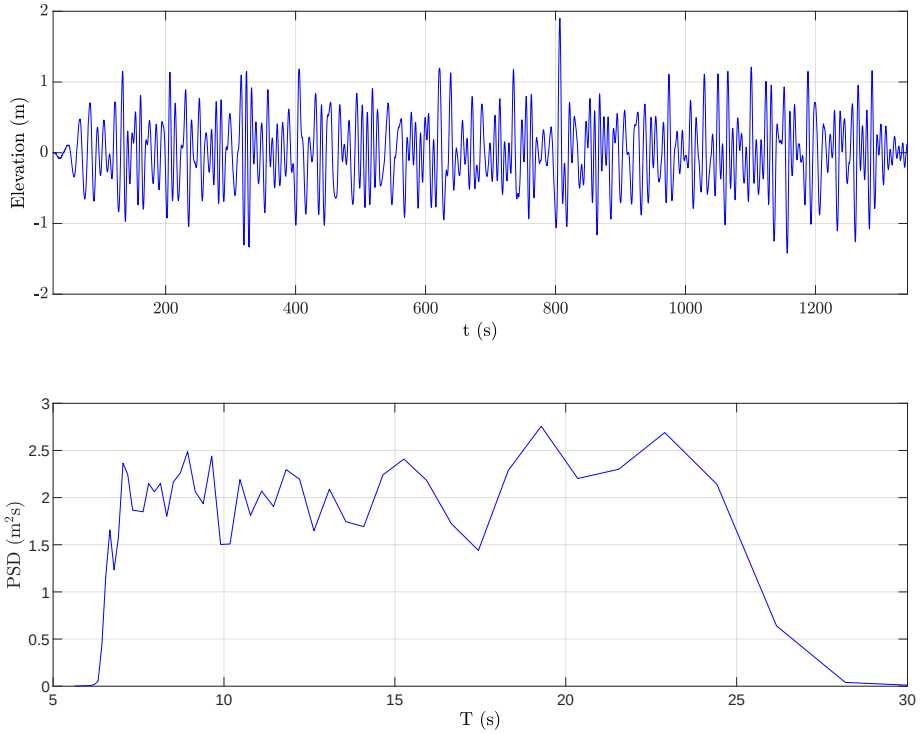

Figure 4. White noise wave characteristics

2.4. Wind actuator

The characterization of the actuator for the calibration of the aerodynamic thrust was performed in a fixed bench (Fig. 5). The input command of the ESC is in PWM (pulse width modulation) that varies from 0 to 100% of thrust. A load cell measured the thrust force, providing the data required to derive the calibration curve relating PWM and to thrust. A typical response curve is shown in Fig. 6, with thrust force in model scale. The signal patch that is highlighted in red marks the sample range used for computing the mean force for that specific PWM value. A non-negligible rise time of approximately 0.8s can be observed in the measurement, but one must remind that, in this case, the propeller starts from rest, whereas during the experiments in waves the dynamic modulation of thrust occurs around a mean value, with variations that are generally only a small percentage of the mean thrust.

To attest that time-delays would not undermine the rotor effects in the wave tests, a second set of bench experiments was done in which the input signal generated by the BEMT routine in the white-noise wave tests was used to measure the actuator response. The BEMT was adjusted to execute wind speed of 11.6 m/s. Fig. 7 shows the thrust time traces for two test repetitions. A fair reproduction of the forces was observed during the whole experiments. The difference of the force measured by the load cell and the required one was generally below 10 kN with peaks of 20 kN (0.019 N and 0.039 N in model scale, respectively), for mean thrust of more than 600 kN. Another result observed is the frequency response of the actuator. In Fig. 8, the transfer function could be observed as a bode plot in the range of the white-noise wave energy, from 0.0385 Hz to 0.15 Hz. It is notable that the phase is not shifted in high frequencies. It remains in a band of 10 deg apart from the input command. The magnitude loss was reasonably adjusted to an exponential decay-like exp(-2.9*f). However, it is possible to note that in the low frequency range, corresponding to periods higher than 20 s, the actuator loss is negligible.

Preprints (www.preprints.org) | NOT PEER-REVIEWED | Posted: 5 January 2021 doi:10.20944/preprints202101.0071.v1

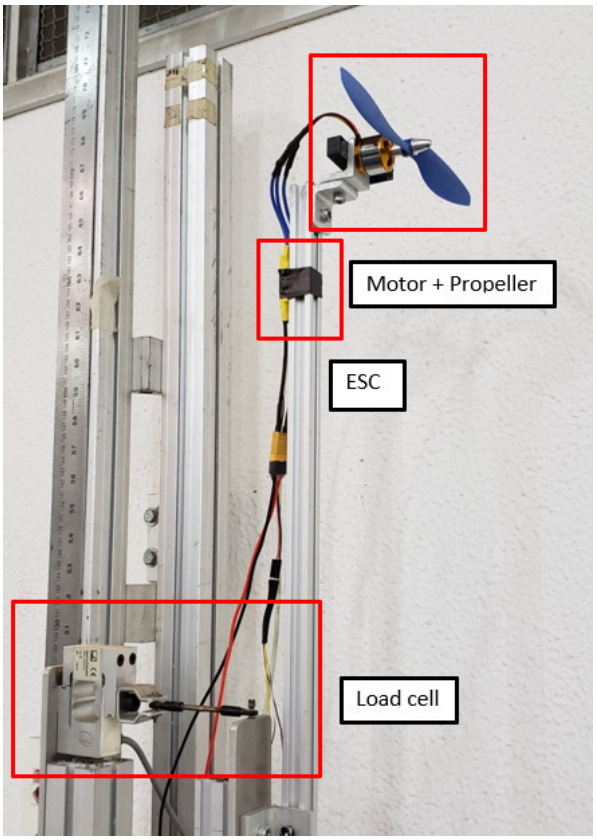

Figure 5. Bench calibration of wind thrust actuator.

2.5. Wind turbine characterization

The NREL 5MW reference wind turbine [17] was considered in the tests. Two different wind velocities were tested: 7.8 m/s (intermediate condition in the power output curve) and 11.6 m/s (maximum thrust force). The optimized power output curve of the turbine is shown in Fig. 9.

It is important to mention that no active rotor control effects were considered during the tests. The rotor speed is taken as constant for each wind velocity and no changes of blade-pitch are modeled, even for the higher wind velocity (11.6 m/s). The variations of thrust therefore arise exclusively from the change of the apparent wind velocity induced by the tower motions.

2.6. Numerical model

The Jappaku floater dynamics in waves was numerically evaluated in frequency domain using the well-known panel method software WAMIT®. Hull geometry and mass/inertia matrix were computed using Edtools® as a pre-processor, by modeling simple parametric structures. In the numerical mesh, hull columns were represented by high-order surfaces, while the heave plates were modeled using dipole panels with zero-thickness. Fig. 10 brings the panels limits adopted for the WAMIT® mesh. In addition, the linearized external mooring stiffness was taken into account considering the 6 dof, with the stiffness matrix computed by means of the analytical formulation proposed by [18]. As it will be shown in Section 3, the mooring system stiffness dependency on both the floater mean position and the mean attitude of the platform (trim/heel) had to be considered for a proper modeling of the motions. Finally, as the viscous effects were not evaluated by the potential theory used by WAMIT®, external linearized damping matrix is required.

For computing the effects of the rotor forces in frequency-domain, a linearized approach already applied by [11] and [12] was adopted. Considering the thrust force represented in Eq. 1, and observing that the apparent wind speed at the rotor axis results from the composition of the steady wind V_w and

Preprints (www.preprints.org) | NOT PEER-REVIEWED | Posted: 5 January 2021 doi:10.20944/preprints202101.0071.v1

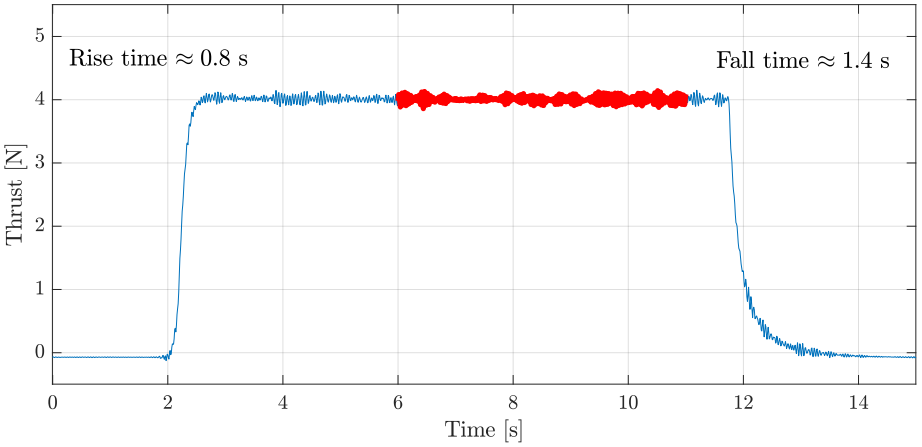

Figure 6. Typical actuator step response of 6000 RPM.

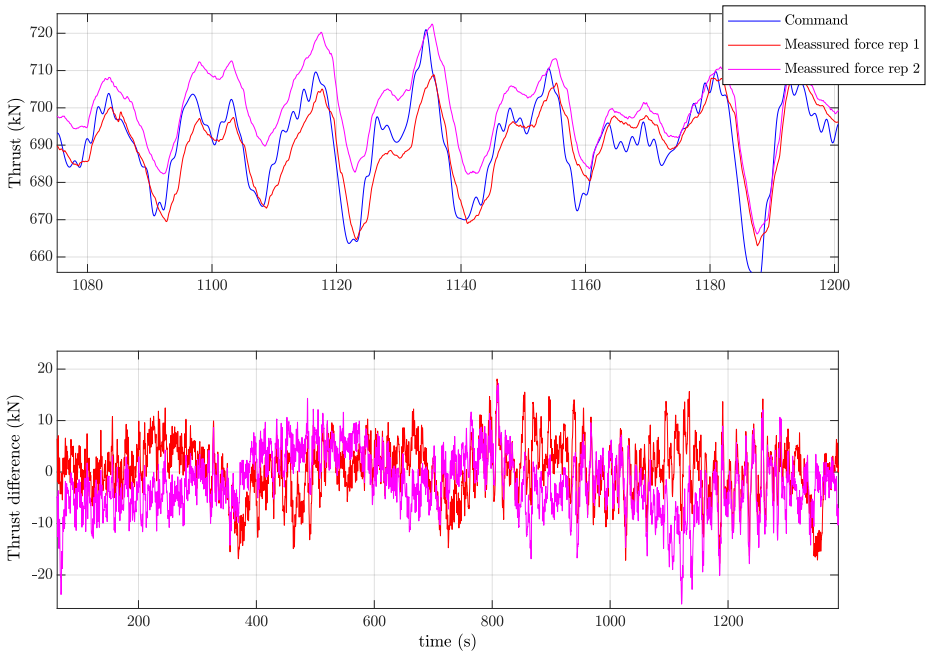

Figure 7. Time domain response of wind thrust actuator.

the periodic velocities induced by the floater surge X_1 and pitch X_5 motions at the nacelle (Eq. 3), it is possible to relate the thrust fluctuations to the rigid-body velocities and, consequently, to the floater RAOs (Eq. 4). Assuming that the variations of rotor thrust are instantaneous (meaning that there are no phase shifts as the ones that might be produced by the changes in blade pitch), the rotor forces are in phase with the floater velocities and can be interpreted as an (external) aerodynamic damping. In the results that will be presented in the next section, the effects of this damping on the floater pitch motions were considered by taking the external damping coefficients B51 and B55 into consideration in the WAMIT model.

$$F_{Wind} = \frac{1}{2}\rho A c_t V^2 \tag{1}$$

being Ac_t the turbine area and V the apparent wind speed, and:

$$V = V_w + i\omega(X_1 + LX_5) \tag{2}$$

Preprints (www.preprints.org) | NOT PEER-REVIEWED | Posted: 5 January 2021 doi:10.20944/preprints202101.0071.v1

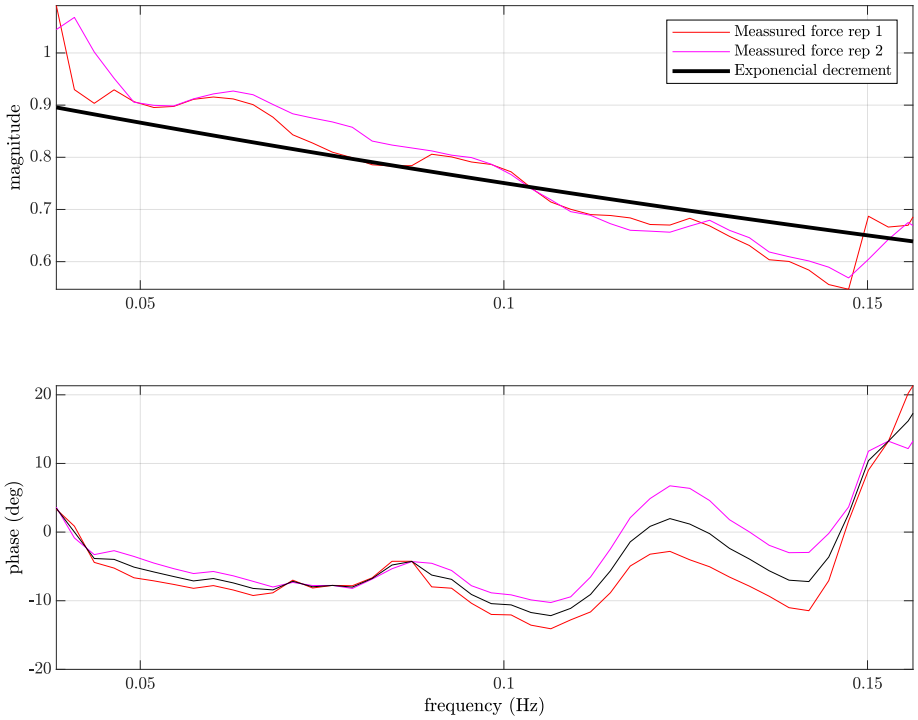

Figure 8. Frequency domain response of wind thrust actuator.

with V_w being the wind speed.

$$F_{Wind} = \bar{F}_{wind} + \left.\frac{\partial T}{\partial V}\right|_{V_w} \left(\dot{X}_1 + L\dot{X}_5\right) \tag{3}$$

being T the thrust force and L the distance from CG to nacelle.

$$F_{Wind} = \bar{F}_{wind} + C_{Wind} i\omega \left(X_1 + LX_5\right) \tag{4}$$

with:

$$C_{Wind} = \frac{1}{2}\rho A \left.\frac{\partial c_t}{\partial V}\right|_{V_w} V_w^2 \tag{5}$$

and c_t the thrust coefficient.

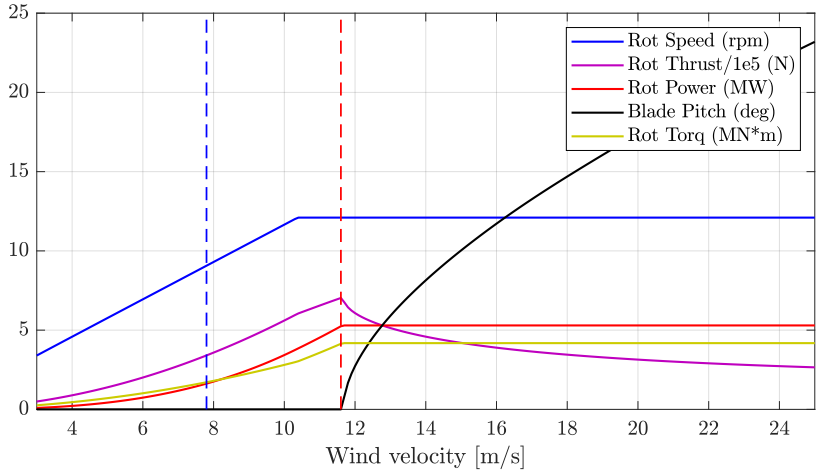

Figure 9. Wind turbine response curve.

Preprints (www.preprints.org) | NOT PEER-REVIEWED | Posted: 5 January 2021 doi:10.20944/preprints202101.0071.v1

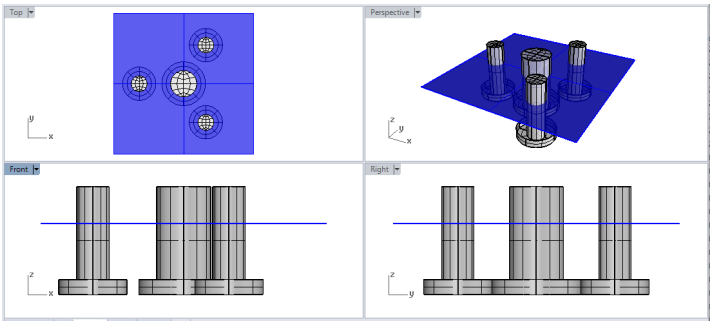

Figure 10. High-order mesh of columns and heave plates - Even keel.

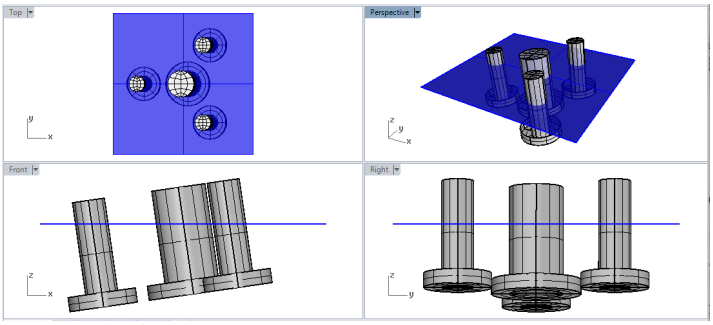

Figure 11. High-order mesh of columns and heave plates - Heeled.

Considering the values of the coefficient $C_{Wind} = 84\ kN/(m/s)$, the damping coupling terms can be defined as $B_{ext51} = C_{Wind}L = 7.3e3kN.s$ and $B_{ext55} = C_{Wind}L^2 = 6.4e5kNm.s$.

3. Results and Discussions

This section presents the main experimental results and discusses the numerical modeling required in order to properly recover them. Firstly, the effects of wind forces on surge, heave and pitch natural periods obtained from decay tests are investigated and comments on the hull mean position and attitude are drawn. Response in waves are presented in subheading 3.2, aiming to study the concomitant effect of not aligned wave and wind. For the present study, the difference of incidences is 30°, as presented in Fig. 12.

3.1. Decay tests

Decay tests were carried out in order to assess natural periods and damping levels. Three wind velocities were considered: no wind, $v_w = 7.8$ m/s and $v_w = 11.6$ m/s. In addition, two different initial inclination angles of the floater were taken into account: even keel and +5° trim. Hereafter, the latter condition will be denoted by "with trim adjustment (TA)". It was adopeted in the tests in order to reduce the mean tilt angles for $v_w = 7.8$ m/s and $v_w = 11.6$ m/s wind conditions, thus emulating the effects of a ballast compensation. Tab. 4 presents the mean surge and mean trim angles for both conditions, with and without TA.

Table 3. Surge, heave and pitch natural periods for each wind condition.

Wind velocity (m/s)	**Periods (s)**			
	T1	**T3**	**T5**	**T5***
0	97.0	16.2	27.6	27.9
7.8	99.6	16.2	24.5	-
11.6	102.8	16.0	22.6	24.6

(*) Adjusted trim - Initial value: +5°

Preprints (www.preprints.org) | NOT PEER-REVIEWED | Posted: 5 January 2021 doi:10.20944/preprints202101.0071.v1

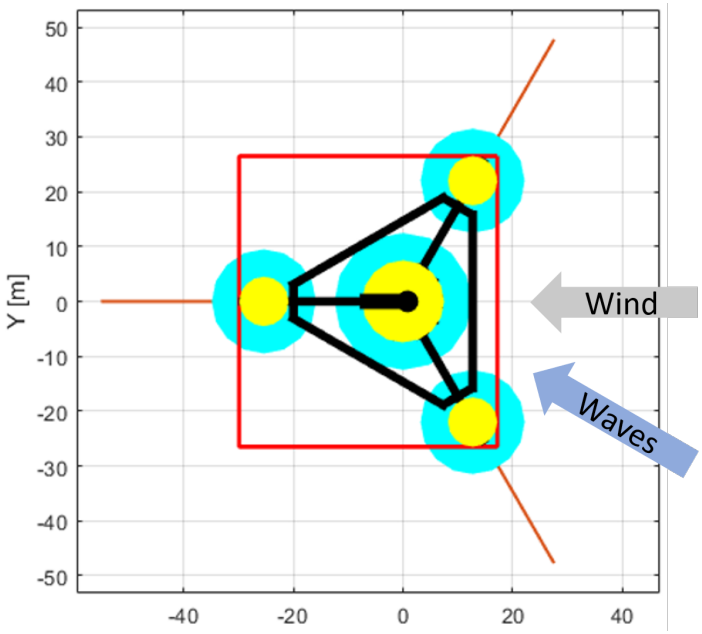

Figure 12. Wind and wave incidences with respect to the Jappaku Hull.

Table 4. Mean surge and hull trim for different wind conditions with and without trim adjustment (TA).

Wind velocity (m/s)	Mean surge		Mean trim angle	
	Without TA	With TA	Without TA	With TA
0	0.0 m	0.0 m	0.0°	5.0°
7.8	-5.1 m	-5.8 m	-4.2°	0.5°
11.6	-10.3 m	-11.1 m	-9.2°	-3.9°

The wind thrust force induces significantly changes in the surge and pitch natural periods obtained from the decay tests. In fact, similar results are found in the literature [12,19,20]. However, the origins of surge and pitch shifting in period are different. Due to the mean thrust load, the FOWT platform drifts to a mean point far from the trivial unloaded position. As discussed by [21] and [18], the new equilibrium position changes the mooring system stiffness, mainly for horizontal motions, as they are the most affected by mooring restoring forces. Fig. 13 brings the stiffness-offset relation, considering different tilt angles of the floater. As a consequence of this change, the natural periods also change. Tab. 5 presents the comparison between the natural periods estimated from the decay tests and those predicted by the numerical model. Mass/inertia and hydrostatic stiffness matrices were computed using Edtools® with added mass matrix obtained from WAMIT®.

Table 5. Surge, heave and pitch natural periods for each wind condition (without trim adjustment).

Wind velocity (m/s)	T1		T3		T5	
	Experimental	Numerical	Experimental	Numerical	Experimental	Numerical
0	97.0	97.6	16.2	16.4	27.6	28.1
7.8	99.6	100.7	16.2	16.4	24.5	28.0
11.6	102.8	103.3	16.0	16.2	22.6	27.6

Numerically obtained natural periods present a fair agreement with experimental results for surge and heave motions, but the same cannot be said regarding the pitch motion. For surge motion, WAMIT model with the adjusted mooring stiffness (from 62 kN/m to 56 kN/m) predicts quite well the physical model response. In Fig. 13, it is notable how the mean offset and attitude of the system change the stiffness coefficients, with the offset, being the principal reason for period changing. On the

Preprints (www.preprints.org) | NOT PEER-REVIEWED | Posted: 5 January 2021 doi:10.20944/preprints202101.0071.v1

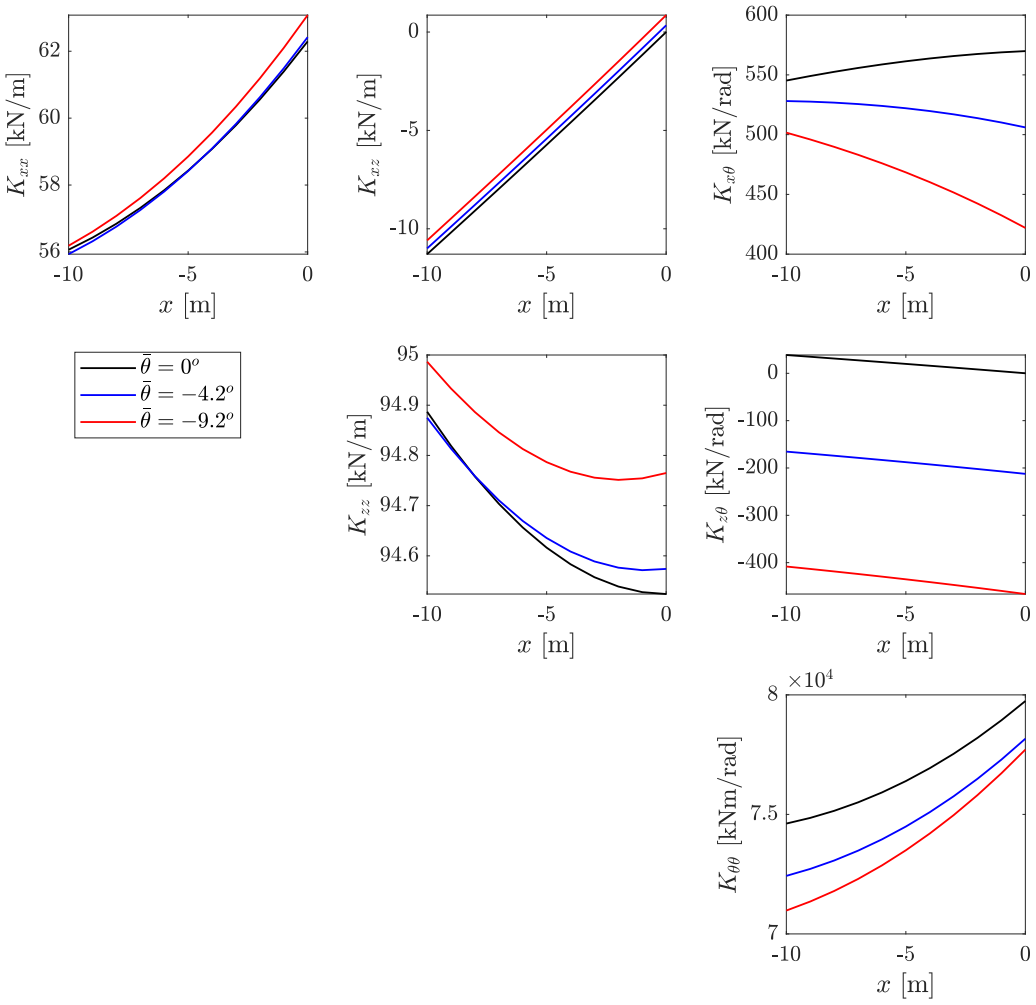

Figure 13. Mooring system stiffness coefficients as functions of surge offset and mean trim.

other hand, changes in the mooring stiffness or phase shifts of the rotor loads do not seem to explain the reduction observed for the pitch period and further investigation on this issue is needed.

Finally, Tab. 6 brings the values the linear and quadratic damping derived from the decay records together with the values of the linearized damping coefficients. The linear and linearized dampings are expressed as a percentage of the critical damping for each dof, while the quadratic damping coefficients are presented as a percentage of the mass/inertia of the respective dof. The estimation of the damping levels followed the procedures presented in [22]. It is notable that thrust force increases the surge and pitch damping ratios. This effect is even more pronounced in the latter. Regarding the quadratic terms, the damping coefficient B_2/M (i.e. proportional to the square of the velocity) is the most affected by the increase of wind velocity. For the linearized damping model, the result indicates that the linearized damping ratio also grows with the wind velocity for surge and pitch, but remains practically unchanged for heave motion. It is important to emphasize that the results present similar trends concerning the ones presented by [12].

3.2. Responses in waves

For assessing the concomitant effects of wind and waves, Response Amplitude Operator (RAOs) were derived from the experimental white-noise wave test. Fig. 14 depicts the heave and pitch RAOs, for all three wind conditions that were tested: no wind, $v_w = 7.8$ m/s and $v_w = 11.6$ m/s. Only the cases without trim adjustment (TA) are shown.

Preprints (www.preprints.org) | NOT PEER-REVIEWED | Posted: 5 January 2021 doi:10.20944/preprints202101.0071.v1

Table 6. Surge, heave and pitch linear and quadratic, and linearized damping ratios for each wind condition.

Wind velocity (m/s)	T1			T3			T5		
	Quadratic		Linear	Quadratic		Linear	Quadratic		Linear
	$\zeta(\%)$	$B_2/M(\%)$	$\zeta_l(\%)$	$\zeta(\%)$	$B_2/M(\%)$	$\zeta_l(\%)$	$\zeta(\%)$	$B_2/M(\%)$	$\zeta_l(\%)$
0	2.0	6.7	5.6	0.3	18.1	2.9	0.6	3.7	2.9
7.8	4.0	7.8	8.8	0.3	16.6	2.7	6.5	4.1	7.5
11.6	5.5	7.3	9.4	0.8	13.3	2.6	6.9	15.4	13.6

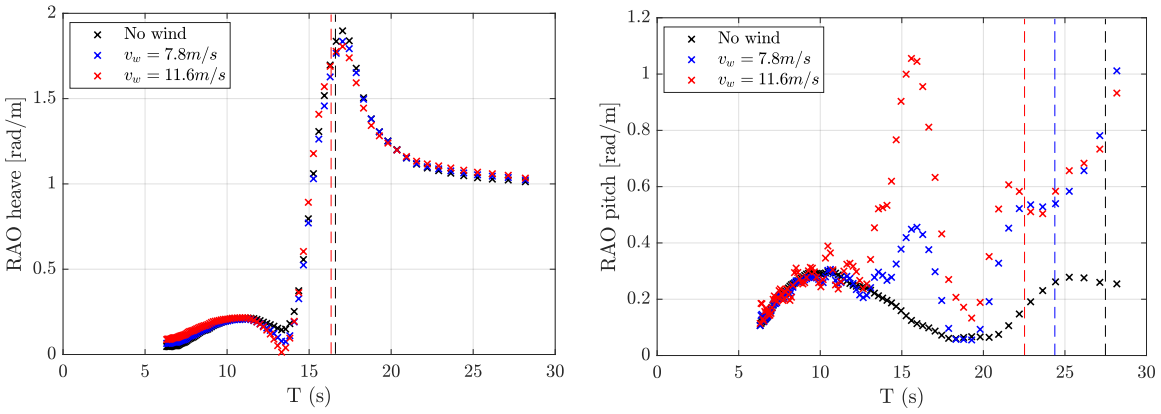

Figure 14. Concomitant effects of wind and waves for different wind velocities: (a) heave and (b) pitch. Dashed lines represent natural periods from decay tests.

It can be noticed that the pitch RAO changes substantially with the wind thrust, similarly to what could be inferred from decay tests. It is also remarkable that the pitch response for the conditions with wind in Fig. 14(b) present an additional peak at T≈ 16 s (i.e. near heave natural period) when compared to the no wind case, pointing to a relevant coupling effect between heave and pitch. Furthermore, a significant increase in the resonant response can be readily identified.

The reasons for the heave-pitch coupling were first investigated experimentally. For this, the two trim conditions presented in Tab. 4 are considered: with and without TA. Fig. 15 brings pitch RAO for wind velocities $v_w = 7.8$ m/s and $v_w = 11.6$ m/s. Mean trim angles for both velocities are shown in the legend.

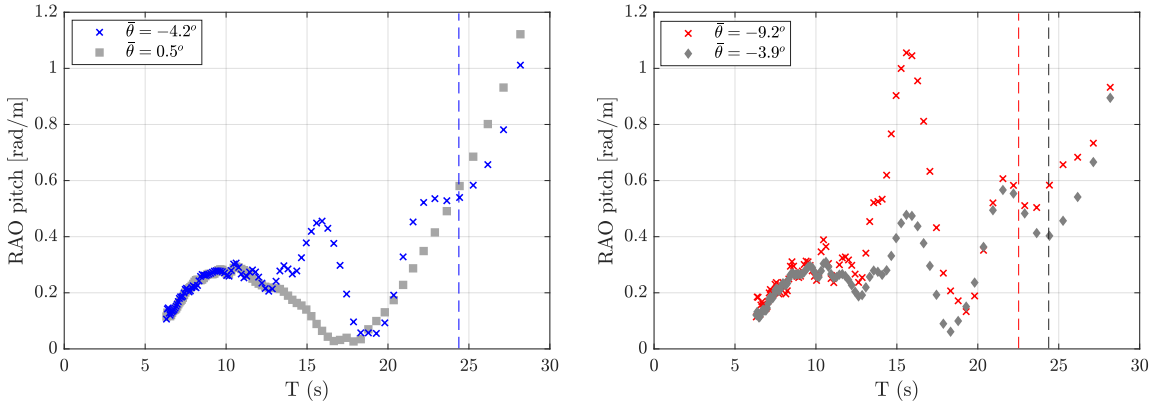

Figure 15. Concomitant not aligned wind and waves for: (a) $v_w = 7.8$ m/s and (b) $v_w = 11.6$ m/s. Dashed lines represent natural periods from decay tests.

Preprints (www.preprints.org) | NOT PEER-REVIEWED | Posted: 5 January 2021 doi:10.20944/preprints202101.0071.v1

By comparing the results, it is possible to realize that the effect induced by ballast changing is remarkable, especially in Fig. 15(a), as the adjusted trim for $v_w = 7.8$ m/s leads to a pitch response that is almost the same observed for the no wind condition. From Fig. 15(b), it is possible to conclude that the heave-pitch coupling increases significantly with the mean trim angles.

In order to better comprehend the behavior of the wave test, the different tilt conditions of the floater for $v_w = 11.6$ m/s were introduced in the hydrodynamic model. For that, two numerical meshes were constructed: one in even keel condition and another with the proper mean trim $\bar{\theta} = -9.2$. Fig. 16 brings the comparison between the numerical predictions with both meshes and the experimental heave and pitch RAOs. It is important to highlight that the proper mooring system stiffness was considered for the WAMIT® model.

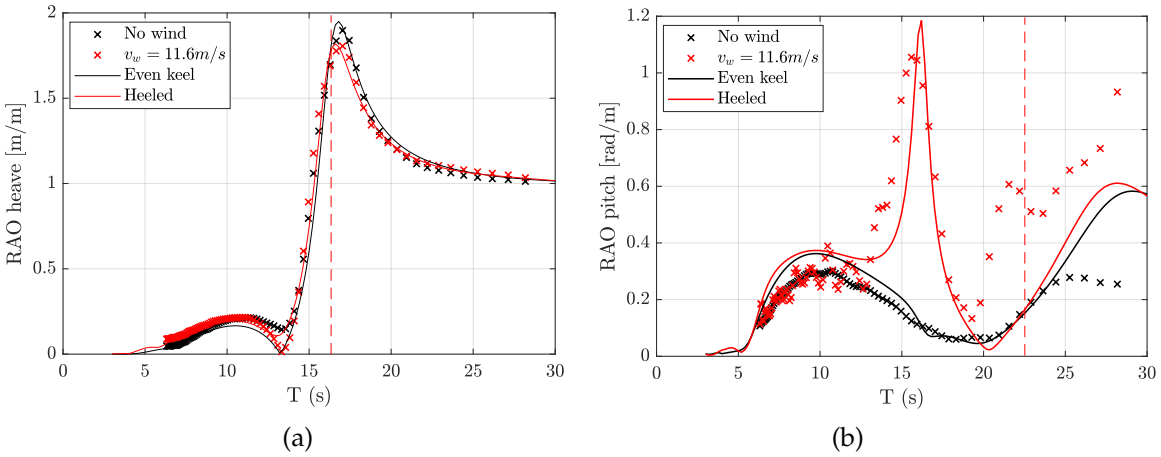

Figure 16. Numerical and experimental RAO for concomitant wind and waves for $v_w = 11.6$ m/s: (a) heave and (b) pitch. Dashed lines represent natural periods from decay tests.

From Fig. 16(b), one may conclude that the mean potential effects arising from the hull trim are indeed the main responsible for the appearance of the additional peak near the heave natural frequency. The changes can be interpreted as a measure of the relevance that a proper ballast control may have on the response of this kind of structure or, alternatively, a measure of the inaccuracies that my be involved in the modelling of this kind of system if larger tilt angles are tolerated in their design.

Finally, it must be emphasized that the effects induced by the trim angle is also responsible for part of the change observed in the resonant range, but it is not sufficient to recover the motion amplitudes and the shifting in terms of period and canceling frequency.

A second step for the numerical modeling was then the proper calibration of external damping coefficients, both from aero and hydrodynamic sources, specially the off-diagonal terms that model coupling effects. It is well known that surge and pitch motions are highly coupled for this kind of structure, but the experiments indicate that external heave-pitch damping coefficients are also relevant once trim angles are significant, and only by tuning both surge-pitch and heave-pitch damping coefficients it was possible to reproduce the cancellation point and peaks observed in the experiment, as illustrated by Fig. 17. The main hypothesis for the heave-pitch external damping term is that it is due to viscous drag, which is not computed by a potential flow tool such as WAMIT. By modeling the structure with Morison's elements and linearizing the quadratic drag force with the statistical linearization method [23], it was possible to obtain the necessary values to match the experimental results. However, this procedure is still in an initial stage of development, requiring a more thorough validation in order to be trustworthy. This topic is currently being analyzed and is expected to be published soon.

Finally, Fig. 18 presents the numerical model calibration versus the experimental data. The red cross marks are the experimental curve for the model with the turbine on at the 11.6 m/s wind speed.

Preprints (www.preprints.org) | NOT PEER-REVIEWED | Posted: 5 January 2021 doi:10.20944/preprints202101.0071.v1

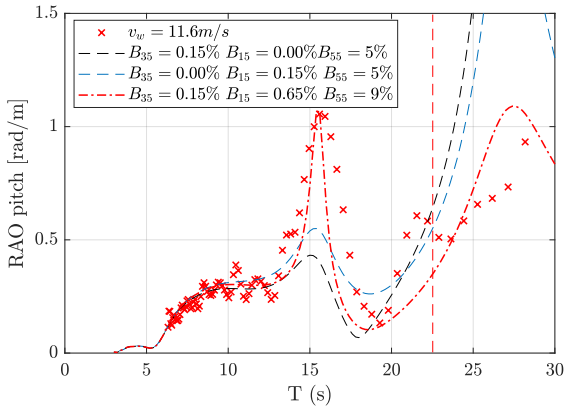

Figure 17. Numerical damping calibration.

The black curve is the numerical model with the even keel configuration. The red line is the model heeled at the angle of 4 degrees due to the turbine moments.

The region close to wave periods of 15s is mopstly affected by the heel angle, while for periods above 20s up to the pitch natural period the aerodynamic rotor coupling is more important. The response in this region also suffers a great influence of viscous damping terms and, therefore, different adjustment would be needed for different wave heights.

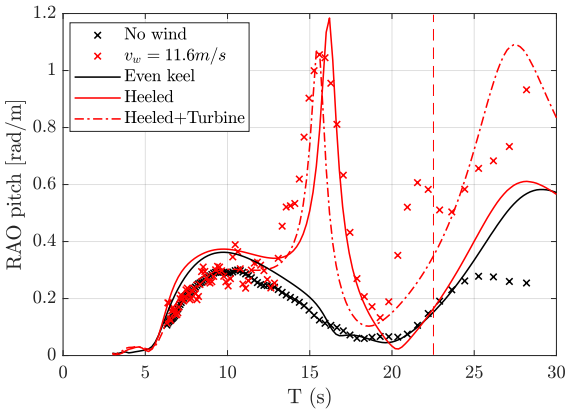

Figure 18. Final numerical model calibration versus experimental data. Dashed lines represent natural periods from decay tests.

4. Conclusions

A series of wave basin results was presented, in which a particular FOWT concept with semi-submersible substructure was tested under waves and wind conditions, the latter being emulated by means of a wind actuator/propeller. No active blade pitch control was included in the tests, but the fluctuations of the rotor thrust induced by the floater motions were predicted and reproduced by the actuator during the tests by means of a SIL scheme. The model drifts were restrained by a set of three catenary mooring lines, with anchors placed at the basin floor. The test conditions induced different tilt levels to the floater, which were only partly compensated by ballast adjustment or not compensated at all, leading to a rich scenario in which different combinations of mean offset, floater tilt, rotor thrust and wave loads were tested.

Decay tests in still water were conducted for conditions with and without wind, rendering the effects of rotor thrust on the resonant periods of oscillation evident. The changes were particularly significant for the surge drift (supposing collinear wind and floater motions), for which a considerable

 doi:10.20944/preprints202101.0071.v1

reduction of the natural period was observed. This was in line with previous observations made in the literature, and it was possible to demonstrate that the main cause for this change was due to the (nonlinear) variation of the mooring stiffness induced by the floater offset from its neutral position, mainly for surge motion. In turn, pitch motion shift in periods seem to result from couplings with other motions, caused by both hydro and aerodynamics. Relevant changes in the level of surge and pitch damping due to the aerodynamic damping produced by the rotor were also observed in the decay tests.

Tests for characterizing the FOWT first-order motion response in waves comprised regular and transient wave tests, and the results obtained with both methods were coincident. The motions recorded during the transient tests with and without wind loads allowed for the estimation of the motion RAOs for a large range of wave frequencies. In a general way, the rotational dofs of motions in the vertical plane (for the test conditions, particularly the floater pitch motions) were the only ones susceptible to significant impacts regarding their dynamic responses in the wave-frequency range. Still, the changes in the pitch response were substantial and, considering that this is one the motions that causes more concern regarding the turbine operation, an effort was made in order to identify the main causes of variation and quantify their impacts.

First of all, it is important to mention that no important changes on the pitch motions came from the catenary mooring lines. Floater tilt, on the other hand, did induced significant impacts. The most relevant part of this impact was characterized by an increase in pitch amplitudes in a range around the heave resonant period. In fact, although the floater counts with heave plates installed on the bottom of each column, a considerable amplification of heave still occurs in resonance (natural period around 16s), with a peak RAO of approximately 2.0 for the wave conditions that were tested. Part of this impact on the pitch RAO could be reproduced simply by re-running the WAMIT® code with a tilted mesh, without further modifications. In fact, the changes in the potential added-masses and radiation damping induced by the floater inclination accounted for a considerable part of the changes observed in the pitch motions, especially due to the coupling between heave and pitch. However, if no further changes were made, significant discrepancies in the pitch response still remained. They could only be corrected properly by the estimation of an external damping matrix, whose origin is hypothesized to be the viscous drag acting on the floater. An approach based on Morison's equation and statistical linearization has provided a good estimate that reproduced fairly well the experimental results, but since it is still in an early stage of development, a more thorough validation is needed before these results can be deemed reliable.

Finally, the aerodynamic effects imposed by the fluctuations of rotor thrust also had a significant influence, but, as expected, this was only true for the pitch resonant range. In fact, in this set of model tests, the fluctuations of apparent wind speed induced by the nacelle velocities were almost instantly translated into variations of thrust load, i.e., with no significant delay. This was verified in the analysis of the test records and confirmed by a set of tests performed with the wind actuator in a test bench. (Here, it is important to remind that no attempt was made in order to model the blade pitch controller response, which, as shown for example by [12], can induce phase shifts in the thrust fluctuations). Therefore, the effects of the rotor were restricted to an additional damping. This damping was modelled by means of a simple linearized model based on the nacelle velocities and the turbine thrust curve, in the way already proposed by [12]. With this model it was possible to estimate reasonable external values of B51 and B55, which indeed led to a better representation of the pitch resonant amplifications.

In summary, the results above show that the correcting the frequency-domain model that accounts for the FOWT motions in waves may be a hard task, especially if relatively large inclination of the floater is considered acceptable (for example, for concepts with no active ballast compensation). This may be particularly important concerning the parametric optimization of the floater geometry, a procedure that is often envisaged for the early design of such devices. In this case, extra care must be taken for guaranteeing that the inaccuracies in the motion transfer functions do not undermine the

predictions of important quality parameters such as the nacelle accelerations and maximum angles of inclination. However, optimization procedures are not the only concern. In fact, oftentimes the analysis of the sea-keeping behavior of a particular FOWT is performed by means of time-domain simulations that rely on pre-computed hydrodynamics coefficients obtained in frequency domain. Again, as it can be inferred from the results presented above, the inaccuracies in the motion responses may be large due to the nonlinearities induced, for example, by the variations in mooring configuration and inclinations of the floater.

Author Contributions: Conceptualization, A.N.S., E.B.M. and G.R.F.; methodology, E.B.M., G.A.A., I.F.A., L.H.S.C. and P.C.M.; software, E.B.M. and G.A.A.; validation, E.B.M. and G.A.A.; formal analysis, E.B.M. and G.A.A.; investigation, E.B.M., G.A.A., I.F.A. and P.C.M.; resources, A.N.S.; data curation, E.B.M., G.A.A., I.F.A. and L.H.S.C.; writing–original draft preparation, A.N.S., G.A.A. and P.C.M.; writing–review and editing, A.N.S., G.R.F. and R.T.G.; visualization, G.A.A.; supervision, G.R.F.; project administration, G.R.F.; funding acquisition, G.R.F. and A.N.S. All authors have read and agreed to the published version of the manuscript.

Funding: This work was developed in the context of a Brazil-Japan collaborative research project n.88887.153223/2017-00 funded by the Brazilian Coordination for the Improvement of Higher Education Personnel (CAPES) and the Japan Society for Promotion of Science (JSPS).

Acknowledgments: Alexandre Simos acknowledges his Research Grant from the Brazilian National Council for Scientific and Technological Development (CNPq). Lucas H. S. Carmo acknowledges CAPES for his PhD grant (Finance code-001)

Conflicts of Interest: The authors declare no conflict of interest.

References

1. Gonçalves, R. T., Franzini, G. R., Simos, A. N., Neto, A. G., Mello, P. C., Carmo, B. S., Nishimoto, K., Malta, E. B., Vieira, D. P., Carmo, L. H. S., Amaral, G. A., Oliveira, M., Wada, R., Hirabayashi, S., and Suzuki, H. A Brazil-Japan Collaboration on a Conceptual Design of a Floating Offshore Wind Turbine for the São Paulo Coast, In of the 27th International Congress on Waterborne Transportation, Shipbuilding and Offshore Constructions, Rio de Janeiro, RJ, Brazil, **2018**.
2. Mello, P. C., Malta, E. B., da Silva, R. O. P. et al. Influence of heave plates on the dynamics of a floating offshore wind turbine in waves. *J Mar Sci Technol* **2020**.
3. Carmo, L. H. S., Mello, P. C., Malta, E. B., Franzini, G. R., Simos, A. N., Gonçalves, R. T., Suzuki, H. ANALYSIS OF A FOWT model in bichromatic waves: an investigation on the effect of combined wave-frequency and slow motions on the calibration of drag and inertial force coefficients. In *Proceedings of the ASME 2020 39th International Conference on Ocean, Offshore and Arctic Engineering*, **2020**.
4. Sclavounos, P., Tracy, C., Lee, S. Floating Offshore Wind Turbines: Responses in a Seastate Pareto Optimal Designs and Economic Assessment. In *Proceedings of the ASME 27th International Conference on Offshore Mechanics and Arctic Engineering*. Estoril, Portugal, **2008**
5. Hall, M., Brad Buckham, B., Curran Crawford, C. Evolving Offshore Wind: A Genetic Algorithm-Based Support Structure Optimization Framework for Floating Wind Turbines. In *OCEANS'13 MTS/IEEE*, Bergen, Norway, **2013**.
6. Hall, M., Brad Buckham, B., Curran Crawford, C. Hydrodynamics-based floating wind turbine support platform optimization: A basis function approach. *Renew. Energy*. 66. 559–569. **2014**.
7. Azcona, J., Bouchotrouch, F., Gonzáles, M., Garciadía, J., Munduate, X., Kelberlau, F., Nygaard, T. A. Aerodynamic Thrust Modelling in Wave Tank Tests of Offshore Floating Wind Turbines Using a Ducted Fan. *Journal of Physics: Conference Series*, 524, **2014**.
8. Battistella, T., Paradinas, D. D., Urbán, A. M., Garcia, R. G. High Fidelity Simulation of Multi-MW Rotor Aerodynamics by Using a Multifan. In *ASME 2018 37th International Conference on Ocean, Offshore and Arctic Engineering*. Madrid, Spain. **2018**.
9. Azcona, J., Bouchotrouch, F., Vittori, F. Low-frequency dynamics of a floating wind turbine in wave tank–scaled experiments with SiL hybrid method. *Wind Energy*. 22(10). 1402–1413. **2019**.
10. Urbán, A. M., Guanche, R. Wind turbine aerodynamics scale-modeling for floating offshore wind platform testing. *J. Wind Eng. Ind. Aerodyn*. 186, 49–57. **2019**.

11. Jonkman, J.M. Influence of control on the pitch damping of a floating wind turbine. In *Proceedings of the ASME Wind Energy Symposium*. **2008**.
12. Souza, C. E., Bachynski, E. E. Changes in surge and pitch decay periods of floating wind turbines for varying wind speed. *Ocean Engineering*, *180*, 223–237. **2019**.
13. Technomar. EdtoolsX Users's manual. **2020**.
14. Mello, P.C., Carneiro, M.L., Tannuri, E.A. et al. A control and automation system for wave basins. *J Mechatronics (Oxford)* **2013**. *23*, 94–107.
15. Ning, A. A Simple Solution Method for the Blade Element Momentum Equations with Guaranteed Convergence. *Wind Energy* **2014**. 1327–1345.
16. Pegoraro, B. Modelagem aerodinâmica de turbinas eólicas flutuantes (in Portuguese). Master of Science Thesis. In *Escola Politécnica da Universidade de São Paulo* **2020**.
17. Jonkman, J., Butterfield, S., Musial, W., Scott, G. Definition of a 5-MW Reference Wind Turbine for Offshore System Development. In *Technical report number NREL/TP-500-38060 - National Renewable Energy Lab. (NREL)* **2009**.
18. Amaral, G. A. Analytical Assessment of the Mooring System Stiffness. Master of Science Thesis. *Escola Politécnica da Universidade de São Paulo* **2020**.
19. Goupee, A.J., Kimball, R.W., Dagher, H.J. Experimental observations of active blade pitch and generator control influence on floating wind turbine response. *Renew. Energy* **2017**, *104*, 9–-19.
20. Bachynski, E.E., Thys, M., Sauder, T., Chabaud, V., Saether, L.O. Real-time hybrid model testing of a braceless semi-submersible wind turbine. Part II: experimental results. In *Proceedings of the ASME 2016 35th International Conference on Ocean, Offshore and Arctic Engineering*, Busan, Korea. **2016**.
21. Pesce, C. P., Amaral, G. A. and Franzini, G. R. Mooring system stiffness: a general analytical formulation with an application to Floating Offshore Wind Turbines. In *Proceedings of the ASME 2018 1st International Offshore Wind Technical Conference*, San Francisco, CA, USA, **2018**.
22. Malta, E. B., Gonçalves, R. T., Matsumoto, F. T., Pereira, F. R., Fujarra, A. L. C., and Nishimoto, K. Damping Coefficient Analyses for Floating Offshore Structures. In *Proceedings of the ASME 29th Internatiional Conference on Ocean, Offshore and Arctic Engineering*, Shanghai, China, **2010**.
23. Silva, L. S. P., Morishita, H. M., Pesce, C. P. and Gonçalves, R. T. Nonlinear analysis of a heaving point absorber in frequency domain via statistical linearization. In *Proceedings of the ASME 2019 38th International Conference on Ocean, Offshore and Arctic Engineering*, **2019**.